Simulation of Airborne Transport and Dispersion for Urban Waterside Releases

TALMOR MEIR,[a] JULIE PULLEN, AND ALAN F. BLUMBERG

Stevens Institute of Technology, Hoboken, New Jersey

TEDDY R. HOLT

Marine Meteorology Division, Naval Research Laboratory, Monterey, California

PAUL E. BIERINGER AND GEORGE BIEBERBACH JR.

Aeris LLC, Louisville, Colorado

(Manuscript received 28 December 2015, in final form 15 September 2016)

ABSTRACT

Results are presented from a tracer-release modeling study designed to examine atmospheric transport and dispersion (''T&D'') behavior surrounding the complex coastal–urban region of New York City, New York, where air–sea interaction and urban influences are prominent. The puff-based Hazard Prediction Assessment Capability (HPAC, version 5) model is run for idealized conditions, and it is also linked with the urbanized COAMPS (1 km) meteorological model and the NAM (12 km) meteorological model. Results are compared with ''control'' plumes utilizing surface meteorological input from 22 weather stations. In all configurations, nighttime conditions result in plume predictions that are more sensitive to small changes in wind direction. Plume overlap is reduced by up to 70% when plumes are transported during the night. An analysis of vertical plume cross sections and the nature of the underlying transport and the dispersion equations both suggest that heat flux gradients and boundary layer height gradients determine vertical transport of pollutants across land–sea boundaries in the T&D model. As a consequence, in both idealized and realistic meteorological configurations, waterfront releases generate greater plume discrepancies relative to plumes transported over land/urban surfaces. For transport over water (northwest winds), the higher-fidelity meteorological model (COAMPS) generated plumes with overlap reduced by about one-half when compared with that of the coarser-resolution NAM model (13% vs 24% during the daytime and 11% vs 18% during the nighttime). This study highlights the need for more sophisticated treatment of land–sea transition zones in T&D calculations covering waterside releases.

1. Introduction

A series of urban tracer-release studies in the United States in the early 2000s resulted in detailed knowledge of dispersion patterns in Oklahoma City, Oklahoma (Allwine et al. 2002); Salt Lake City, Utah (Allwine and Flaherty 2006a); and New York City (NYC), New York (Allwine and Flaherty 2006b, 2007). These large field and modeling studies illuminated the complicated pathways of horizontal and vertical transport in urban environments in summertime and have led to advances in numerical transport and dispersion (''T&D'') models to more faithfully represent features of the urban environment. In particular, the urban treatment has been examined and enhanced within the Hazard Prediction Assessment Capability (HPAC) software—the tool that is used in national and international response. Hanna and Chang (2012) showed that the Urban Dispersion Model (UDM) integrated into the HPAC software improved the agreement with tracer observations. Additional detailed T&D model evaluations for Salt Lake City (Warner et al. 2004a; Chang et al. 2005), Oklahoma City (Hanna et al.

[a] Current affiliation: Verisk Analytics, Inc., Jersey City, New Jersey.

Corresponding author address: Talmor Meir, Stevens Institute of Technology, Castle Point Terrace, Hoboken, NJ 07030.
E-mail: tmeir@stevens.edu

DOI: 10.1175/JAMC-D-16-0025.1

2008, 2011), and NYC (Hanna et al. 2009; Hanna and Chang 2015) utilized HPAC and demonstrated its appropriateness for simulating urban releases.

The 2005 NYC deployment of the U.S. Department of Homeland Security (DHS)–Defense Threat Reduction Agency (DTRA) Urban Dispersion Program (UDP) involved sulfur hexafluoride and perfluorocarbon tracer releases in the vicinity of Madison Square Garden and Rockefeller Center, two interior sites of midtown Manhattan. NYC is fundamentally a coastal city, with the Hudson, East, and Harlem Rivers flowing through the New York–New Jersey (NY–NJ) region as they merge into the coastal Atlantic Ocean waters of the New York Bight. Although it was originally envisioned, the UDP did not end up conducting tracer releases to measure and map the transport near water.

In a recent study, Rodriguez et al. (2013) developed a method to examine HPAC plume sensitivity to ambient wind direction on a generic urban grid. Their approach quantifies how deviations in wind and release location at street level translate into sensitivity of contaminant concentration footprints. Their results motivated the consideration here of the sensitivities induced by changes in surface characteristics—namely, urban/land and water.

The study that is presented here investigates the meteorological contribution (by both near-surface observations and models) to T&D plumes in the urban–coastal setting of the NY–NJ region. Once an air pollutant is released into the atmosphere, chemical, microphysical, and meteorological factors determine how it is distributed. Here we will investigate the meteorological influences only.

Meteorological conditions determining the concentration of air contaminants in urban–coastal settings differ from those of inland urban regions because of the influences of sea and land breezes, among other factors. Bornstein (1968) showed that winds undergo three-dimensional deformations in urban settings such as NYC. Indeed, weather patterns have been shown to deflect or bifurcate around cities (Gedzelman et al. 2003; Bornstein and Lin 2000). Therefore, to correctly characterize urban–coastal meteorological influences on T&D processes, a three-dimensional consideration of the environment is essential (Brown 2004).

Meteorological-model horizontal resolution is extremely important in coastal areas, where the temporal and spatial inhomogeneity of the wind and turbulence fields can vary substantially (Mahrer and Pielke 1977). Meir et al. (2013) established that a high-resolution meteorological model incorporating an urban parameterization can capture mesoscale processes (resulting from surface heating, terrain forcing, and turbulent mixing) and also possesses the advantage of representing the nuances of land–sea boundaries in the NY–NJ region. In particular, Meir et al. (2013) showed that predictions from the 1-km NYC Coupled Ocean–Atmosphere Mesoscale Prediction System (COAMPS[1]) agreed well with observed near-surface winds for the coastal areas in and around NYC during summer months. The high-resolution meteorological model captured dynamic sea-breeze fronts—meteorological processes of temporally short duration that have a large impact on the region during early summer months.

This study will examine T&D patterns, both horizontally and vertically, and document heat flux distributions as well as atmospheric boundary layer (BL) stability as they pertain to air–sea–land transition regions. The primary tool used in this study is HPAC, a standard T&D model. HPAC was developed by DTRA (DTRA 2008; Sykes et al. 2007). In October of 2012, the DHS Interagency Modeling and Atmospheric Assessment Center designated DTRA as the Chemical, Biological, Radiological, Nuclear, and Explosive Technical Operations Hub for national incidents. In this role, HPAC has been employed in numerous operational incidents nationally, in addition to its use by the U.S. Defense Department worldwide. HPAC has been utilized extensively by the research community and has been evaluated against field-study measurements, as highlighted previously.

Here HPAC is used to simulate releases from four different sites, under three different wind regimes, during the day and at night and driven by different meteorological sources [mean/normal climatological conditions (hereinafter ‘‘climatology’’), meteorological stations, and meteorological models] as discussed further in the methods section (section 2). The current study 1) examines the capability and limitations of an integrated system of meteorological and T&D models on a local scale, 2) seeks to improve the understanding of local atmospheric circulations that are influenced by urban–coastal zones and their physical constraints on airborne contaminant transport, and 3) maps potential sites of interest for future studies and deployment of additional measurements.

The methods section describes the meteorological sources used in HPAC and the hierarchy of meteorological specifications used in our studies, along with the release scenario and statistics used to quantify percent overlaps and over/underpredictability of the plumes. The results section (section 3) discusses different case

[1] COAMPS is a registered trademark of the Naval Research Laboratory.

studies: 1) T&D sensitivity to variations in wind direction as based on climatology and station data, 2) specification from meteorological models of increasing degrees of complexity, and 3) the impact of abrupt changes in surface characteristics. The results explore specification of horizontal and vertical meteorological inputs to T&D applications, daytime and nighttime variations, and the manifestation of urban/land–sea boundary surface characteristics in T&D predictions. The analysis considers both the horizontal and vertical BL structure and the resultant transported plumes.

2. Methods

The selected models and implementation strategy are designed to provide a hierarchy of increasing complexity of meteorological specification to a T&D model. Our suite of simulations begins with a spatially uniform wind specification inspired by climatology (mode 1), then utilizes observed winds and temperatures at multiple meteorological stations (mode 2), and finally employs gridded model horizontal (mode 3) and vertical/higher-order fields (mode 4) representing a more consistent atmospheric representation from a coarse-resolution (12 km) model and a fine-resolution (1 km) model. More details of the models, observations, and release scenario are given in sections 2a, 2b, and 2c, respectively. The details of the T&D model implementation are presented in section 2d, and section 2e contains a description of the performance metrics for the T&D model that are employed in the results section.

a. Models

1) Transport and dispersion model

HPAC, version 5.0, is a software system for atmospheric T&D processes. It generates or imports wind fields into a material transport model, Second-Order Closure Integrated Puff (SCIPUFF), which produces an airborne contaminant plume. The model comprises a set of dispersion equations that are based on the Gaussian-puff method (Bass 1980) in which an ensemble of three-dimensional puffs is used to calculate a concentration field, and a turbulent-diffusion parameterization that is based on the second-order turbulence-closure theories of Donaldson (1973) and Lewellen (1977). Within the model, the atmosphere is categorized into two regions: 1) the lower-atmosphere BL, where the wind velocity fluctuations provide the inputs for the turbulence calculations, and 2) the upper atmosphere, where the turbulence description is based on climatological information according to the conditions of the atmosphere. Meteorological inputs are required to run HPAC. The system accepts three different kinds of meteorological input: surface mode, profile mode, or gridded data. HPAC makes use of all provided meteorological input and calculates the remaining parameters on the basis of algorithms that are summarized in appendix A. In our simulations the UDM is activated. Details of the urban options in HPAC can be found in Warner et al. (2006).

2) High-resolution weather model

The NYC urbanized nonhydrostatic COAMPS (Hodur 1997) nested down to 1-km horizontal resolution is used as a source of weather-model input to HPAC. The outer grid's atmospheric forcing is derived from the U.S. Navy Operational Global Atmospheric Prediction System (NOGAPS) model. The ocean surface boundary forcing is the Navy Coastal Ocean Data Assimilation (NCODA) 9-km multivariate optimal-interpolation ocean-state analysis that combines in situ and remotely sensed data (Cummings 2005) on a 12-h update cycle. In this configuration, COAMPS is updated every 12 h and outputs hourly fields on a 91 × 91 grid with 70 vertical sigma levels, where 36 levels are in the lowest 1200 m to allow for greater resolution of BL processes. For vegetated and nonurban areas, the Noah land-surface model (Liu et al. 2006) is used. For urban areas, an urban canopy parameterization scheme that is based on Brown and Williams (1998; BW-UCM) with a rooftop energy equation by Chin et al. (2005) is used. The details of the model configuration have been previously reported in Holt and Pullen (2007) and Thompson et al. (2007). Results from NYC COAMPS simulations using this model configuration were presented and analyzed in Meir et al. (2013).

3) Coarse-resolution weather model

The North American Mesoscale Forecasting System (NAM) is one of the primary models of the National Weather Service Environmental Modeling Center and is currently utilized as a meteorological-model input to DTRA through the Meteorological Data Server. NAM is a nonhydrostatic mesoscale model that has been run for the continental United States at 12-km horizontal resolution since 2006 (Janić et al. 2001). The model was originated by the National Centers for Environmental Prediction and is maintained by the National Center for Atmospheric Research (NCAR). The surface boundary conditions and presence of urban land characteristics are specified as high-density residential land use in the Noah land-surface model (Liu et al. 2006). The NAM forecasting system outputs 3-hourly fields on a 25 × 23 grid. NAM has 39 vertical sigma levels, with 10 levels in the lower 1200 m of the atmosphere.

b. Meteorological station data

The Optical Remote Sensing Laboratory of The City College of New York aggregates meteorological

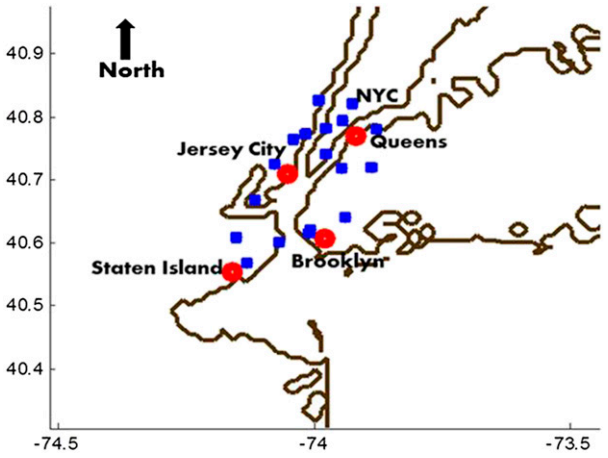

FIG. 1. The 22 land-based near-surface meteorological stations, four of which (marked in red) also correspond to release sites.

observations at high temporal resolution (~15 min) around the NYC metropolitan area as part of MetNet (http://nycmetnet.ccny.cuny.edu/). There are a total of 22 meteorological stations utilized in this study, four of which are also chosen as release sites (Fig. 1). Measurements from the 22 selected sites are taken at ~10-m height.

Late-summer climatological winds for the NYC metropolitan area are generally westerly with a southeasterly component from sea breezes (according to the National Centers for Environmental Information) and vary between day and night (Bornstein and Johnson 1977). Common synoptic conditions consist of warm air masses arriving from the southeast and cold air masses impinging from the northwest (Keim et al. 2005). Multiyear measured August and September wind directions and magnitudes for the Newark, New Jersey, airport station confirm these canonical patterns (Fig. 2).

We consider three typical late-summer/early-autumn wind regimes in NYC. The wind regimes are southwesterly, northwesterly, and southeasterly. In section 3a we examine the impact of small wind direction deviations from these idealized orientations on the plume footprint.

Station-produced 10-m winds across the domain are examined to select dates in August and September of 2014 on which the observed winds at the release sites were from approximately southwest (SW), northwest (NW), and southeast (SE) directions in daytime (1300 local time) and nighttime (0100 local time) (Table 1). Winds were between ~0.5 and 5 $m\,s^{-1}$ during these times, with SE daytime winds being the strongest.

c. *Release scenario*

Four urban–coastal locations in the NYC metropolitan area are used as hypothetical release sites: Jersey City (40.70°N, 74.05°W), New Jersey, and Staten Island (40.55°N, 74.16°W), Brooklyn (40.60°N, 73.98°W), and Queens (40.77°N, 73.91°W), New York (Fig. 1). These sites are chosen for their collocation with meteorological-station measurements and waterfront proximity. All releases are identical and use a 20-m-height aerial spray release of a neutrally buoyant gas with a mass load of 10 kg. The release configuration is designed to highlight processes in the lower BL where buildings in NYC typically reach 20 m (Holt and Pullen 2007). Contaminant regions are analyzed predominantly 2 h after release, using mainly dosage (time integral of concentration) contour level 18 × 10^{-6} $kg\,s\,m^{-3}$, following National Research Council (2001).

d. *T&D model implementation*

T&D patterns in this study are systematically analyzed by varying meteorological inputs from simplest to most

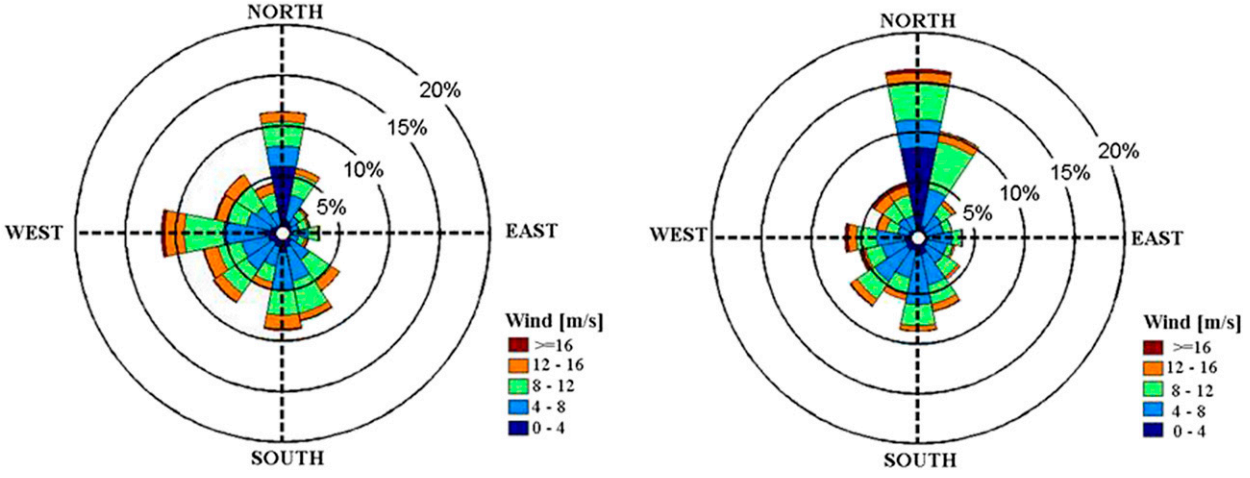

FIG. 2. Wind rose of hourly Newark station data for (left) August and (right) September for 2010–15.

TABLE 1. Observed wind speeds ($m\,s^{-1}$) and directions (°) on days chosen to capture southwest, northwest, and northeast orientations. Day is 1300 and night is 0100 local time.

	SW day: 29 Sep 2014		SW night: 27 Aug 2014		NW day: 26 Sep 2014		NW night: 15 Aug 2014		SE day: 13 Sep 2014		SE night: 22 Aug 2014	
	Speed	Direction	Speed	Direction	Speed	Direction	Speed	Direction	Speed	Direction	Speed	Direction
Jersey City	0.9	190	2.2	222	1.3	86	2.2	345	5.4	120	2.2	160
Staten Island	0.5	288	0.4	263	0.5	312	0.4	248	0.9	115	0.9	118
Brooklyn	1	182	1.5	217	1.5	317	4.6	289	8.7	82	1.5	137
Queens	1.5	199	1	251	2.6	51	1.5	343	2.6	145	0.5	137

complex, as described by the four modes (Fig. 3). Mode 1 consists of a constant wind across the entire grid. HPAC then calculates all other meteorological parameters as constants on the basis of seasonal and stability assumptions (appendix A).

Mode 2 uses wind and temperature observations from 22 near-surface stations from MetNet (Fig. 1). The sensors provide 10-m observed wind and temperature data at the release date/time (Table 1). For each near-surface observation, HPAC calculates wind and turbulence vertical profiles with a total of eight sigma levels, three of which are in the lower 1200 m. HPAC uses the profiles to interpolate winds and turbulence over the entire domain and adjusts according to a canopy parameterization using mass-consistency theory to ensure mass conservation as flow travels around obstacles. (No good-quality measured profile data were available in the region.) For further description of HPAC's built-in equations for developing the wind profiles, see appendix A. In this mode HPAC also calculates a constant heat flux H and BL depth. Mode 2 output is considered to be the "control" plume with which the higher modes are compared in the results section.

Mode 3 uses gridded horizontal meteorological-model wind and temperature inputs at the model resolution (as described in section 2a) at the release date/time. HPAC then calculates a constant H, BL depth, and vertical profiles. Mode 4 employs modeled 3D wind and temperature fields and spatially varying H and BL depth that are also taken from the weather models. That is, HPAC does not compute profiles in mode 4 since they are specified from the meteorological models.

e. Metrics

Predicted plumes resulting from the various meteorological inputs (Fig. 3) are compared using two methods. "Percent overlap" is used to measure the overlap between two individual surface plumes. It is calculated at a fixed time (typically 2 h after a release), for a fixed dosage level (nominally $18 \times 10^{-6}\,kg\,s\,m^{-3}$) and is defined as the ratio of the area of intersection divided by the area of the control plume. In this study, percent overlap will also measure the intersection areas of plumes derived from meteorological-model inputs (COAMPS and NAM) with control plumes that are calculated on the basis of observed near-surface winds and temperatures from station data at 22 sites.

Measure of effectiveness (MOE) is a statistical metric that accounts for the size, shape, and location of the plume (Warner et al. 2004b) and is used to analyze the overlap region. MOE is a two-dimensional technique that differentiates over- and underpredicted areas: the x axis corresponds to the ratio of the overlap region to the control plume, and the y axis corresponds to the ratio of the overlap region to the weather model–derived plume. MOE values along the diagonal of the two-dimensional plot connote equal-sized plumes. A point farther along the diagonal represents larger overlap. A complete overlap of plumes is represented by $x = 1, y = 1$, while $x = 0, y = 0$ denotes no area overlap between the plumes.

3. Results

a. T&D sensitivity to wind orientation

An evaluation of sensitivity to wind direction is conducted on the basis of the method of Rodriguez et al. (2013) and employing the mode-1 meteorological-input

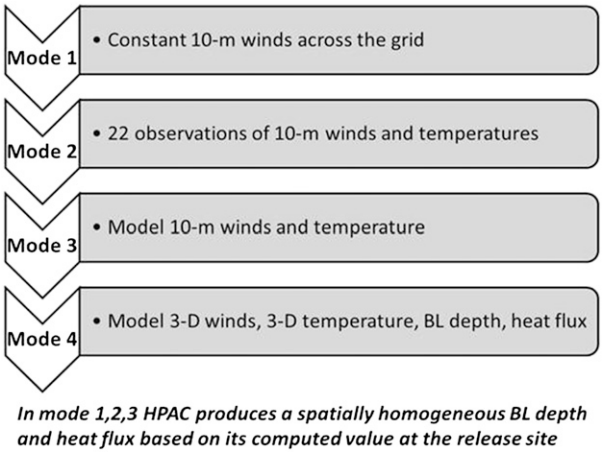

FIG. 3. Hierarchy of meteorological specifications used in the study.

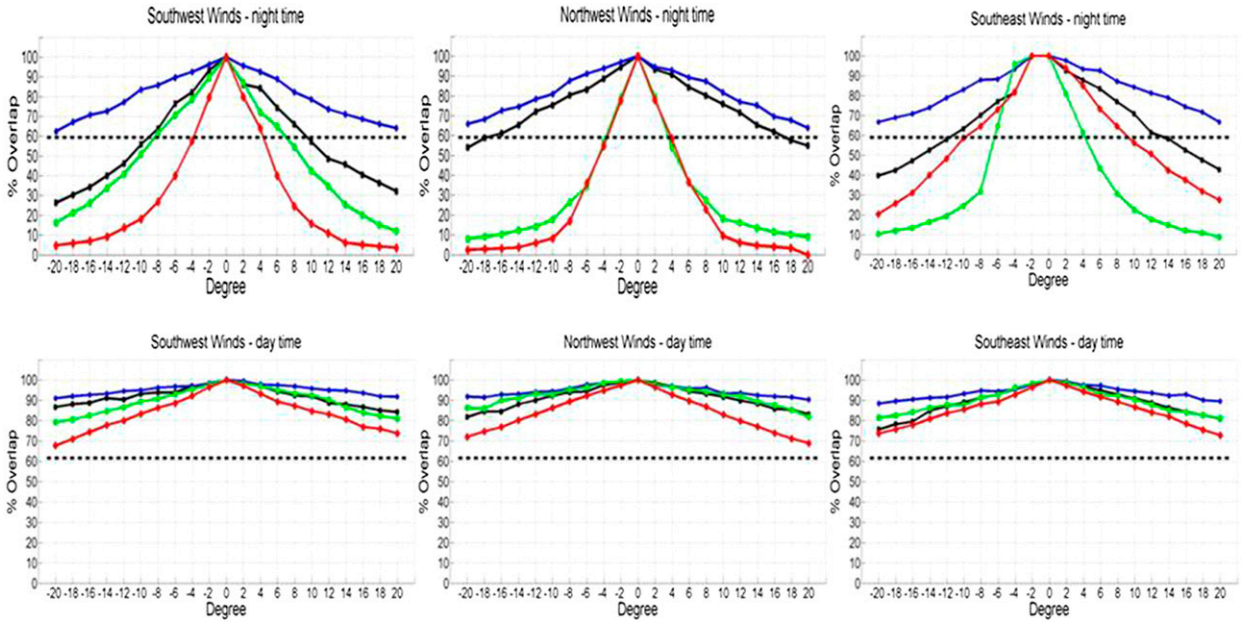

FIG. 4. HPAC plume percent overlap calculated 2 h after release using mode-1 meteorological specification: (top) night releases (0100 local time) and (bottom) day releases (1300 local time). Uniform winds over the domain for base wind directions of southwesterly, northwesterly, and southeasterly are varied in 2° increments to generate plumes. The line colors represent different release sites: red is Jersey City, green is Staten Island, black is Queens, and blue is Brooklyn.

specification to HPAC. Here the method is applied to incremental wind direction variations for the NYC region. Using fixed near-surface winds of 4 m s^{-1} from three base orientations—SW (225°), NW (315°), and SE (135°), we use HPAC to compute plumes for each of the four release sites. Base plumes are then compared (by means of percent overlap) with 20 additional plumes resulting from ±2° incremental deviations in wind direction from the original orientation (10 plumes in the positive direction and 10 plumes in the negative direction).

Overall, an increase in directional deviation resulted in a decrease of percent overlap (Fig. 4), but the results show strong sensitivities to time of day and release-site location. Daytime plumes are less sensitive to wind direction variations (i.e., higher percent overlaps among plumes). For a 20° deviation from northwesterly winds, a daytime minimum of 71% overlap occurred whereas the overlap is reduced to 2.5% at night.

In addition to diurnal differences, a marked increase in T&D plume variability is apparent when plumes are transported over water. The decrease in overlap is sharpest when winds are from the northwest, transporting air directly over water. Over the water, surface roughness is low (see Table A1 of appendix A), influencing the near-surface diffusion within HPAC. This results in elongated and narrow plumes that are sensitive to small wind direction shifts.

Plumes transported over water (from release sites in Jersey City and on Staten Island) show ~80% spread in plume overlaps during nighttime NW winds as compared with sites propagating plumes over land (Brooklyn and Queens) that show only ~40% spread in plume overlaps (Fig. 4). Jersey City and Staten Island are most sensitive to wind direction variations because of the proximity to the coastline and the NY–NJ Harbor waters. By contrast, Brooklyn is an area characterized by dense, low building heights such that any wind direction deviation will continue to transport the plume over the same land-surface characteristics. Hence it shows the most uniformity in plume footprint across the wind variations. The uniform land-surface type of buildings in HPAC also leads to mass-consistency effects that enhance transport and contaminant spread in a spherical pattern that will be discussed more in the next section.

b. T&D sensitivity to meteorological specification

T&D model sensitivity to meteorological inputs is explored next by examining the results of utilizing horizontal and vertical model output. Here we probe the differences in plumes arising from specifying near-surface winds and temperatures from 22 meteorological stations (mode 2) as compared with specifying horizontally varying near-surface model winds and temperatures (mode 3) and adding vertical and higher-order model fields (mode 4).

Several case studies that utilize different wind directions are examined. We begin by focusing on a Staten

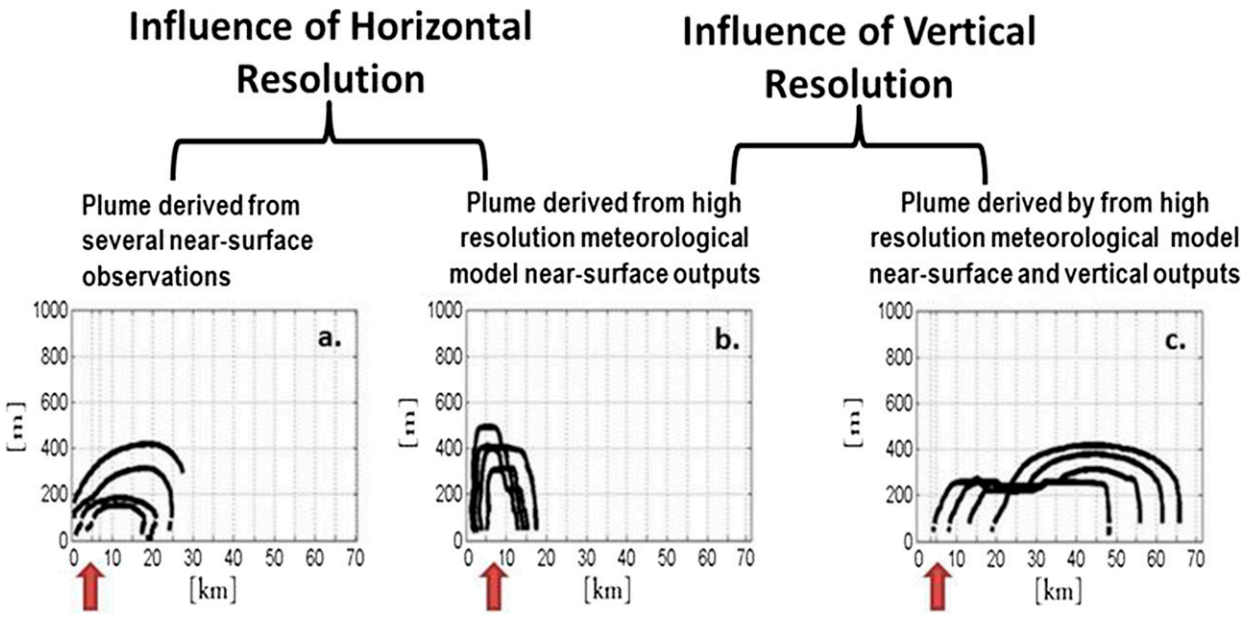

FIG. 5. For the Staten Island release site (marked with a red arrow), vertical concentration in the downwind direction for nighttime plumes derived from (a) near-surface observations (mode 2), (b) COAMPS horizontal fields (mode 3), and (c) COAMPS horizontal, vertical, and higher-order fields (mode 4). Contours are shown 2 h after release, with contour levels at 1×10^{-11}, 1×10^{-13}, 1×10^{-15}, and 1×10^{-17} kg s m^{-3}.

Island nighttime release. Prevailing observed northwesterly winds were chosen (Table 1), and meteorological-model winds for the corresponding date and time were extracted. COAMPS model surface wind bias is $-1.96\,\mathrm{m\,s^{-1}}$. (For additional information, in appendix B near-surface model winds are compared with station wind data at the release sites.)

HPAC plumes that are based on multiple near-surface observations (mode 2; Fig. 5a) and high-resolution (COAMPS 1-km) horizontal meteorological inputs (mode 3; Fig. 5b) simulate similar plume patterns and share 44% horizontal overlap several hours after release. The similar plume pattern is due in part to HPAC's assumption of constant atmospheric stability across the entire grid (on the basis of unvarying values of H and BL depth) and an exponential function for wind profiles if not input. These meteorological simplifications inhibit local turbulence generation, keeping contaminants close to the release site (within 5–10 km downwind). In comparison, providing high-resolution three-dimensional wind fields into HPAC calculations (Fig. 5c) results in strong advection of contaminants out to nearly 60 km in the downwind direction. The T&D plumes from high-resolution three-dimensional wind fields (mode 4) share merely 17% horizontal overlap with those from control mode 2 and 20% with T&D plumes that are derived from high-resolution horizontal meteorological inputs (mode 3). The vertical aspects of plume transport will be investigated in more detail in section 3c.

A coarser-resolution model (NAM) is now included, and results are examined for both day and night releases at multiple locations, focusing on the mode-4 specification. Southwesterly day and night plumes derived from observed near-surface conditions (mode 2), COAMPS 1-km higher-order fields (mode 4), and NAM 12-km higher-order fields (mode 4) are computed (Fig. 6). Meteorological quantities consisting of near-surface winds, H, and BL depth are compared for modes 2 and 4 (Fig. 7 and Table 2).

Daytime plumes result in small, circular-shaped footprints of contaminant on the surface, whereas nighttime plumes are characterized by elongated contours (Fig. 6). Surface winds are responsible for the general direction of the trajectories (Fig. 7), whereas vertical wind gradients (Fig. 8) provide additional control on horizontal advection; H contributes to vertical turbulence, and BL depth determines the extent to which the contaminant will mix vertically into the atmosphere. HPAC's method of turbulence estimation utilizes the convective velocity scale, which is directly related to both the H and BL-depth estimates (from Deardorff 1970; see our appendix A).

During the daytime, strong H ranging up to nearly $270\,\mathrm{W\,m^{-2}}$, in combination with a deep well-mixed

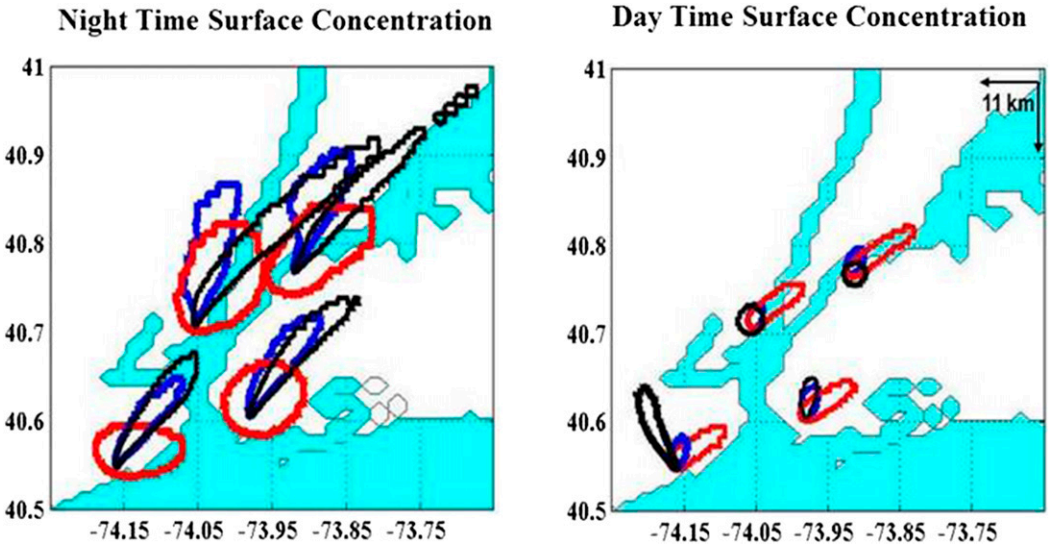

FIG. 6. HPAC plumes 2 h after release derived from near-surface observations (mode 2; red) and higher-order meteorological input (mode 4; COAMPS is black and NAM is blue) for night and day southwesterly winds. The 18×10^{-6} kg s m^{-3} contour is shown.

BL extending over ~2000 m and nearly no vertical wind gradient (Fig. 8), contributes to the quick dilution of the contaminant, thereby reducing the low-level concentration and associated surface dosages. Nighttime releases experience atmospheric conditions that are more stable, where BL depth averaging ~630 m and negligible H values of less than 10 W m^{-2} constrain contaminants to stay close to the ground, inhibiting vertical mixing.

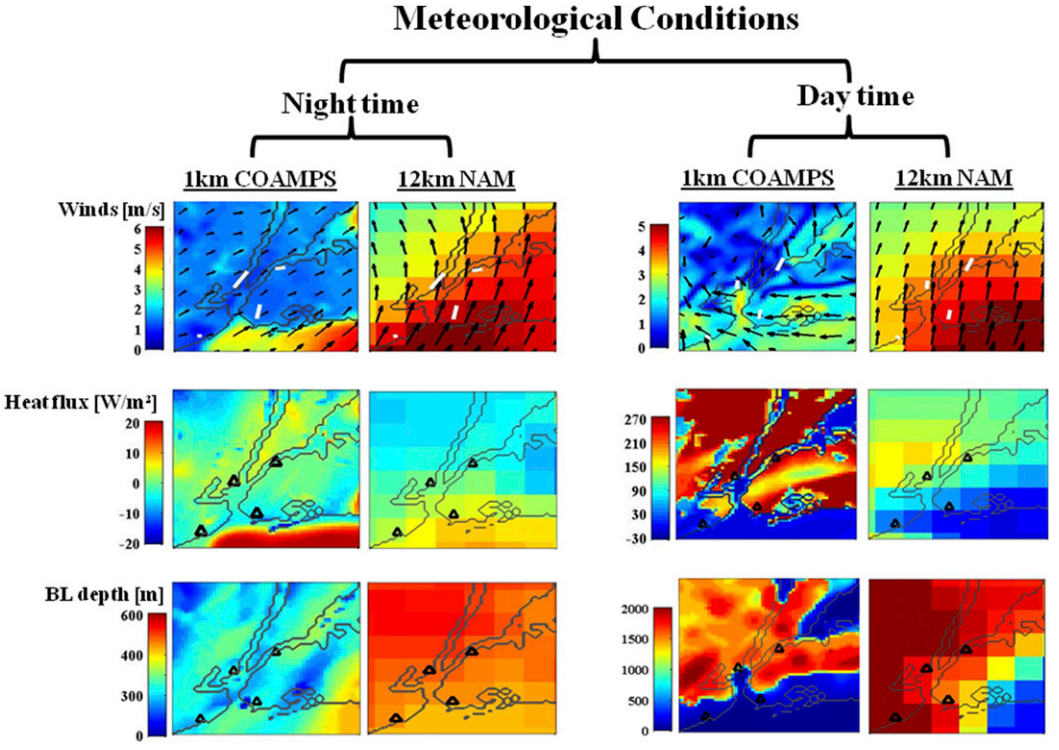

FIG. 7. Surface winds, heat flux, and BL depth from 1-km COAMPS and 12-km NAM (mode 4) at the day and night release times. The white lines show observed winds.

TABLE 2. Heat flux (W m^{-2}) and BL depth (m) calculated by HPAC from observations (mode 2, labeled as Obs in table), 1-km COAMPS (mode 4), and 12-km NAM (mode 4) for daytime and nighttime releases with southwesterly winds. The underlying calculations for these values are explained in appendix A. Here, N/A means that the values are calculated internal to HPAC and are not available for export.

Release site	MET input	Night heat flux	Night BL depth	Day heat flux	Day BL depth
New Jersey	Obs	−8.20	635	N/A	1000
	COAMPS	2.34	253	263	1164
	NAM	0.36	475	112	1642
Staten Island	Obs	−0.05	602	N/A	1000
	COAMPS	−1.73	201	28	68
	NAM	5.59	423	20	2082
Queens	Obs	−0.55	583	N/A	1000
	COAMPS	1.08	251	326	1633
	NAM	−2.89	478	132	1857
Brooklyn	Obs	−2.82	616	N/A	1000
	COAMPS	−4.98	218	242	217
	NAM	4.56	450	28	1347

The sensitivity of horizontal and vertical plume structure to postrelease time is also examined. The time evolution of nighttime plume concentration for the same Staten Island release case of southwesterly winds that is shown in Figs. 6–8 illustrates the plume footprint in the horizontal and vertical directions (Fig. 9). Utilizing only one station for meteorological data (Fig. 9a) leads to a circular plume, which is mildly elongated horizontally when more stations are added (Fig. 9b). In this case, there are three meteorological stations in the vicinity that influence the plume trajectory downwind (Fig. 1). When higher-resolution three-dimensional meteorological fields are added, the plume is substantially elongated in the downwind direction (Figs. 9c,d) and enlarged in the vertical direction (Figs. 9g,h). This effect is exacerbated over time by enhanced atmospheric transport in the model-derived meteorological specification (mode 4). For instance, at 30 min after release, COAMPS (NAM) surface plume areas expand at a rate of 0.46 (0.31) km min^{-1} as compared with the 0.4 km min^{-1} of mode 2. By 2 h after release, COAMPS (NAM) expands at 1.23 (1.01) km min^{-1} as compared with mode 2 at 0.65 km min^{-1}. Areas of overlap exhibit similar patterns, sharing greater overlap 30 min after release relative to 2 h after release.

c. *T&D sensitivity to urban–water boundaries*

The Staten Island release site is examined in more detail for daytime conditions (Fig. 10), where internal

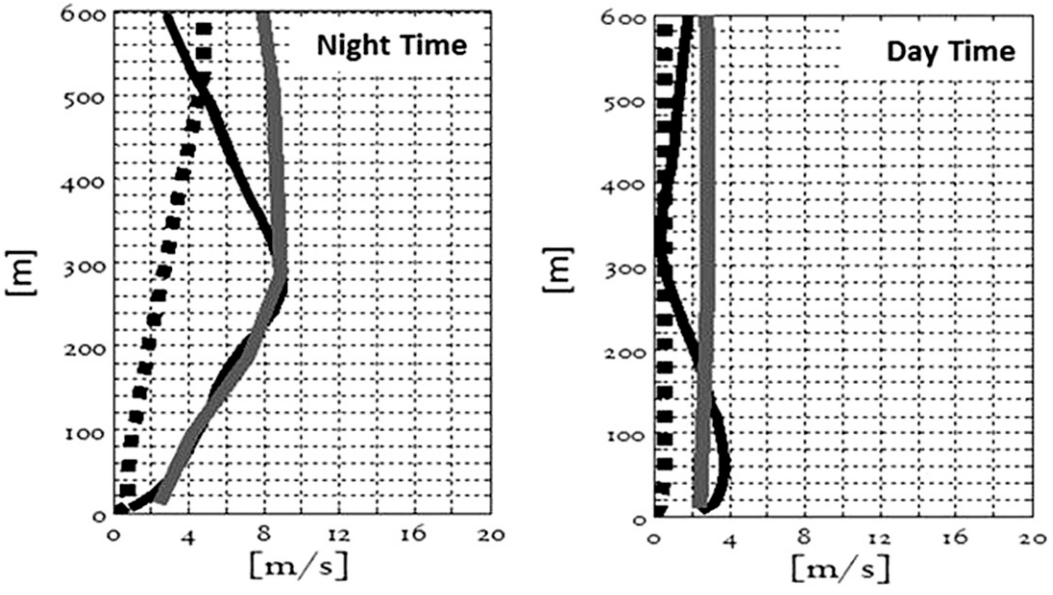

FIG. 8. Computed Staten Island vertical wind fields for southwesterly winds at (left) 0100 local time and (right) 1300 local time. Dashed lines are HPAC calculated fields, solid black lines are COAMPS fields, and solid gray lines are NAM fields.

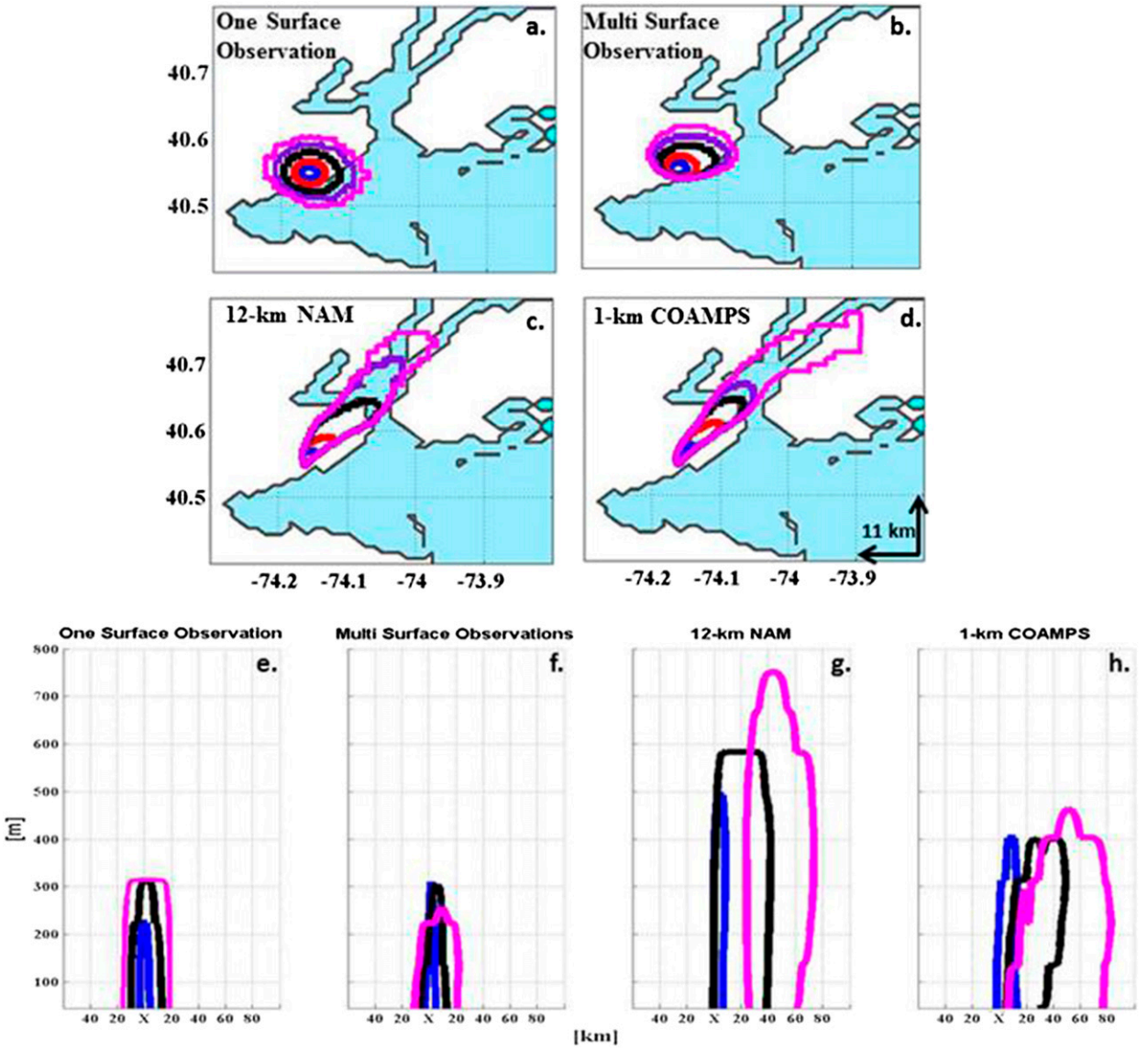

FIG. 9. Time evolution of computed plumes for nighttime southwesterly winds at the Staten Island release site. Postrelease times are shown for 15 (blue) and 30 (red) min and for 1 (black), 1.5 (purple), and 2 (magenta) h. (a)–(d) The 3×10^{-7} kg s m^{-3} [shown for graphical clarity and corresponding to a mild dosage effective on 10% of the population (ECt10), for reference] horizontal contour. (e)–(h) The 1×10^{-14} kg s m^{-3} vertical contour. The meteorological specification are mode 1 for (a) and (e) mode 2 for (b) and (f), and mode 4 for (c),(d),(g), and (h).

BL formation in the vicinity of the NY–NJ Harbor was simulated by high-resolution COAMPS (Fig. 10c). Southeasterly winds over NY–NJ Harbor advect colder marine air associated with small H and shallow BL depth. The coastal atmospheric structure around Staten Island is initially dominated by marine influences ($H \sim 28\,\mathrm{W\,m^{-2}}$ and BL depth = 68 m). Farther inland, the atmosphere slowly adjusts to the new underlying land-surface characteristics ($H \approx 210\,\mathrm{W\,m^{-2}}$ and BL depth $\approx$ 2000 m). Incorporating the meteorological input of an internal BL (as described above) into T&D calculations results in a unique vertical distribution of the contaminant across the transition zone in the downwind direction (Fig. 10). This feature was not captured by the coarser-resolution NAM model. It is useful to resolve these small scales (or even smaller ones) in this coastal area. Upwelling zones in summertime can form along New Jersey and the Long Island south shore and cause atmospheric cooling (Pullen et al. 2007), which, as demonstrated here, directly influences T&D predictions.

White et al. (2009) examined an Oklahoma City release case in which a nearby thunderstorm and front altered the

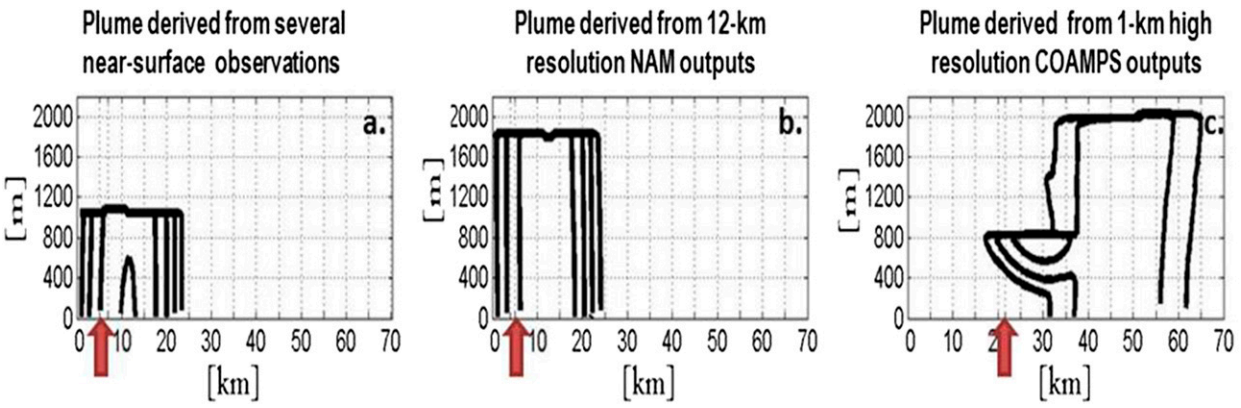

FIG. 10. Staten Island concentration transect in the downwind direction 2 h after release using (a) mode 2, (b) mode 3, and (c) mode 4. The release site is marked with a red arrow.

BL characteristics so much that the HPAC assumptions that were based on near-surface measurements were rendered inaccurate. For that case as well as this case, surface heat fluxes play an important role in modulating T&D properties. The treatment of heat fluxes as well as the need for more vertical information (profile measurements) is warranted to enhance plume fidelity.

An explicit investigation of T&D behavior over urban/land and sea is carried out through a hypothetical release at the coastal Staten Island site during a summer night with NW prevailing winds. Contaminant plumes and meteorological variables are evaluated along a northwest–southeast cross section A–B (shown in Fig. 11) at the overland Staten Island release site, 5 km downwind (over water), and 15 km downwind (over water).

The summer nighttime temperatures over the NY–NJ Harbor water are ~5°C warmer than adjacent land-surface temperatures (Meir et al. 2013). In HPAC, surface H gradients are primarily manifestations of sea surface temperature, which in turn drives atmospheric vertical turbulence patterns that transport plumes vertically into the atmosphere. COAMPS calculates an H of 45.4 W m^{-2} and a 219-m BL-depth gradient over the 15-km A–B cross section, NAM calculates an H of 6.5 W m^{-2} and a 156-m BL-depth gradient, and an H of 0 W m^{-2} and 0-m BL depth is calculated by HPAC, which maintains constant H and BL-depth values for the entire grid in mode 2 (Table 3). As a result of strong H gradients and growing BL depths, NAM and COAMPS (mode 4) produce strong dilution accompanied by vertical transport, as shown in the zoomed-in depiction of the vertical concentration slices of Fig. 12. The contaminant plumes derived from NAM meteorological fields lift the plume to ~20 m above ground, and those from COAMPS lift it to ~40 m above ground. HPAC's internal calculations and lack of input meteorological variation across the grid in mode 2 result in plumes that are confined closer to the ground.

d. *Synthesis statistics*

From the results so far, and similar to the sensitivity study in section 3a, daytime releases produced greater agreement among the plumes across all locations (Table B1 of appendix B). The 1-km COAMPS-derived (mode 4) plumes average 33% overlap with station-driven (mode 2) plumes during the daytime as compared with 13% overlap at nighttime; 12-km NAM-driven (mode 4) plumes average 40% daytime overlap against 17% overlap at nighttime.

Simulations for daytime southeasterly winds, for which contaminants are transported mainly over land, produced the largest fractional overlap across all sites, averaging 70% overlap for COAMPS-derived plumes and 58% overlap for NAM-derived plumes (Table B1, below). For COAMPS-generated day plumes, the Staten Island and Jersey City release sites, under SE winds, have the greatest percent overlap with the control plumes. This result is attributable to a combination of daytime BL structure, land-surface friction, and turbulence, as explained previously. The modeled southeasterly surface winds also have the least directional bias relative to observations.

Simulations for daytime northwesterly winds, mostly transporting plumes over water, lead to the least percent overlap, with COAMPS and NAM-derived plumes having an average across all sites of 13% and 24% overlap, respectively. For COAMPS, the New Jersey and Staten Island release locations in this wind regime have the overall lowest percent overlaps with the control plumes.

The enhanced sensitivity of releases transported over water is also exhibited in the MOE statistics (Fig. 13). Nighttime COAMPS- and NAM-produced

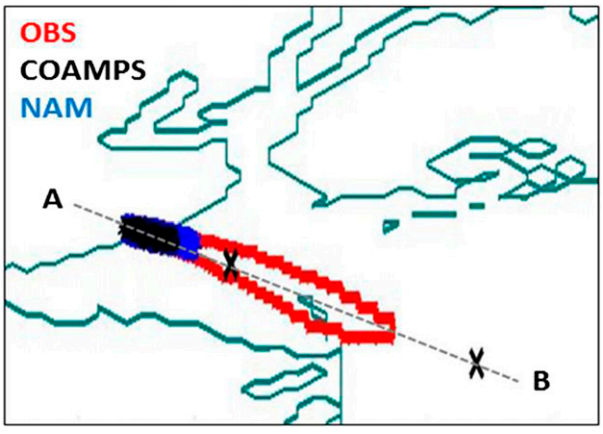

FIG. 11. Staten Island nighttime northwest-wind release conditions, showing the 18×10^{-6} kg s m^{-3} contour 2 h after release along the northwest–southeast cross section A–B. Marked with a cross are the land-based Staten Island site (mostly obscured), a point that is 5 km downwind, and a point that is 15 km downwind.

plumes systematically underpredict the plume hazard area relative to the control plumes for all wind directions selected. Daytime plumes show a marked distinction between COAMPS and NAM specification. COAMPS SE plumes overpredict whereas NW plumes underpredict hazard areas. This result can be attributed to the more sophisticated treatment of land surfaces manifested through COAMPS's higher resolution, urban canopy parameterization, and realistic SSTs relative to NAM. These high-fidelity features represent nuances of the land–sea transition region that lead to more disparate plume outcomes relative to the control and to NAM-derived plumes.

In the aggregate, as based on size, shape, and location, 90% of the meteorological-model-driven plumes underpredict the hazardous area of the contaminant relative to the mode-2 meteorological specification. Indeed, 95% show less than 50% overlap against meteorological-station-derived plumes using simplified H and BL assumptions (mode 2). False negatives (underestimation of surface dose) are typically tolerated less than false positives (overestimation of surface dose) (Garten et al. 2003).

Analyzing predictions in terms of shape and size rather than in terms of percent overlap reinforces the findings that atmospheric T&D predictions are in better agreement across all meteorological inputs during the day (i.e., more data points in the upper-right-hand side of the MOE graph). MOE statistics also illuminate the discrepancies in the shape of the contaminant footprint between T&D plumes calculated from meteorological-model fields and those calculated from observational inputs during the nighttime. Nighttime releases are more on the left-hand side of MOE plots, indicating that the intersection between the elongated meteorological-model plumes, due to a stable nocturnal atmosphere (section 3b), and the control plumes is a small fraction (~0.2). On the other hand, the intersection is greater in relation to the area of the meteorological-model plumes (y axis). Note that 58% of COAMPS-derived releases share at least 60% of total control-model area and that 90% of NAM's releases have at least 60% shared area. Although there is less agreement in shape among the various plumes (data points are positioned away from the diagonal line), there is general agreement on directionality of the transport of plumes.

MOE analysis adds a new element to previous conclusions showing that the complex surface forcing that is represented on various model horizontal grid resolutions and that utilizes different land-surface schemes results in substantially varying plume shapes and sizes. These effects are highly dependent on the wind orientation and whether the plume is transported over water.

4. Summary and conclusions

This study examined the impact of air–sea–land transitions on T&D predictions in urban–coastal regions. Processes influencing T&D behavior in an urban–coastal environment can vary over short distances (~1 km) because of changing land-cover characteristics, thermally induced turbulence, winds, and time of day. T&D surface plumes using diverse sources of meteorological input are more convergent in daytime when the planetary BL is deep and well mixed, with minimal vertical wind gradient—consistent with prior research. The atmospheric conditions facilitate vertical pathways for pollutant transport, thereby reducing surface dosages

TABLE 3. Heat flux (W m^{-2}) and BL depth (m) estimations for land–sea cross section A–B shown in Fig. 11 (SI = Staten Island, with downwind distance given).

	Calculated by HPAC from obs		1-km COAMPS		12-km NAM	
	Heat flux	BL depth	Heat flux	BL depth	Heat flux	BL depth
SI	2.17	400	−10.16	205	19.51	579
SI + 5 km	2.17	400	27.30	539	24.76	676
SI + 15 km	2.17	400	35.21	424	26.01	735

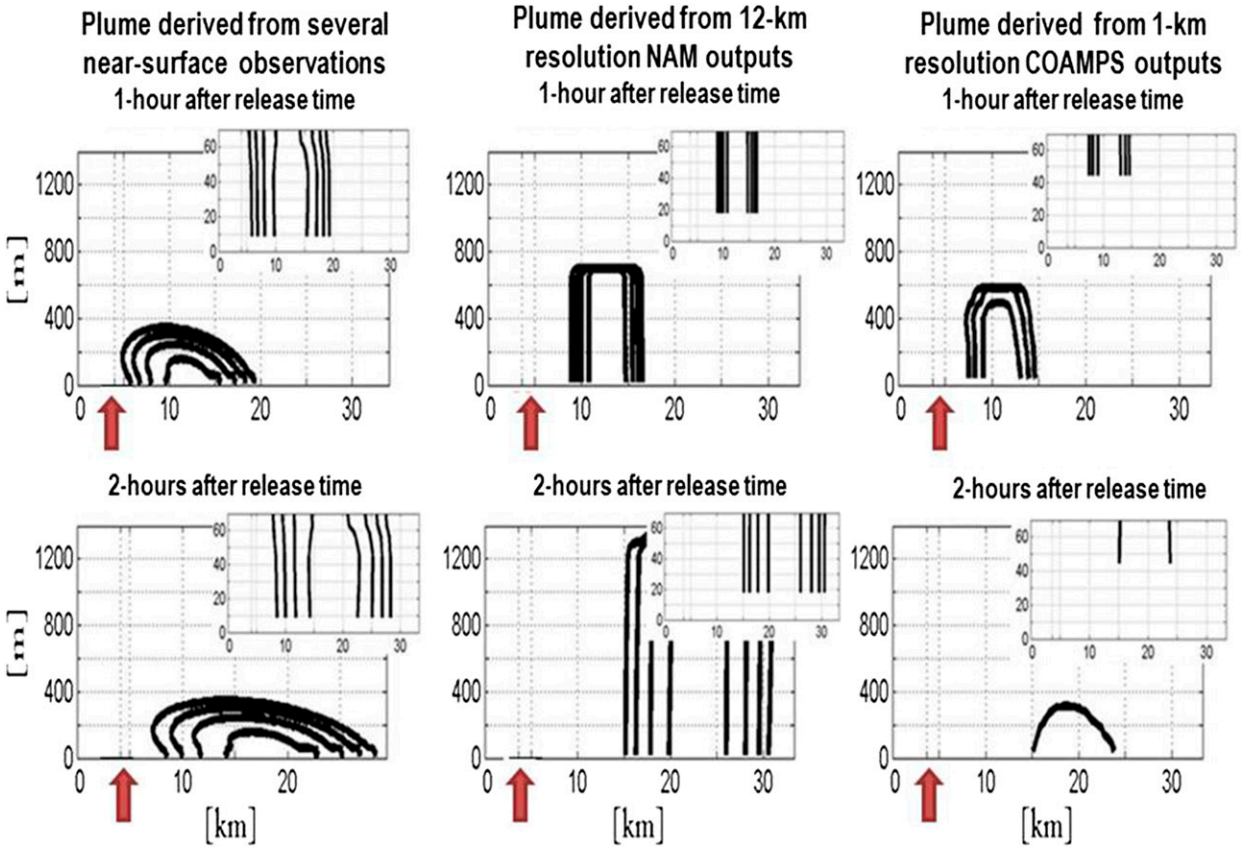

FIG. 12. Staten Island concentration transect in the downwind direction for a release at 0100 local time with northwesterly winds, showing (top) 1 h after release and (bottom) 2 h after release. Insets in the top-right corners of the panels depict near-surface contours. Contours at 1×10^{-11}, 1×10^{-13}, 1×10^{-15}, and 1×10^{-17} kg s m^{-3} are shown for (left) mode 2 and (center) (right) mode 4. The release site is marked with a red arrow.

and increasing percent overlap (70%–90%) among the predictions.

The direction of T&D predictions is sensitive to fluctuating surface wind direction, especially when plumes are transported over the NY–NJ Harbor (section 3a). Moreover, Staten Island showed a strong sensitivity of plume trajectory to small deviations in wind orientation. The site displayed internal boundary layer formation (section 3c) and produced high variability in plume outcomes (section 3d). During the day under southeast winds, plumes encounter homogeneous urban land-surface forcing and tend to share the highest degree of overlap. These distinctions are evident in both COAMPS- and NAM-derived plumes and are magnified when comparing NW and SE winds since NW (SE) winds drive plumes the most (least) over water.

The quality of any T&D model prediction for contaminant concentration levels is highly dependent on the quality of the input meteorological information, as shown here and in other instances (e.g., Garten et al. 2003). We document the plume footprints of diverse meteorological sources in simulations designed with increasing sophistication of meteorological specification, from simple climatology to meteorological-model fields used in operational T&D. Overall, 90% of meteorological-model-driven plumes in this study are estimated to underpredict the hazardous area in comparison with meteorological-station-driven plumes (based on near-surface observations and scale assumptions) (see section 3d). Although station-driven plumes are defined as the control for comparison purposes, they should not be interpreted as truth (section 2d).

The divergence among the predicted hazardous areas suggests the need for an ensemble plume approach to emergency response for complex regions such as coastal NY–NJ (Galmarini et al. 2001). To be more explicit, an ensemble of plumes could be used during nighttime when the atmosphere is more stable, averaging $H < 10\,\mathrm{W\,m^{-2}}$ and 630-m BL depth. In these conditions contaminants remain lower to the ground, subjected to strong vertical wind gradients, thereby resulting in surface plumes with greater spread.

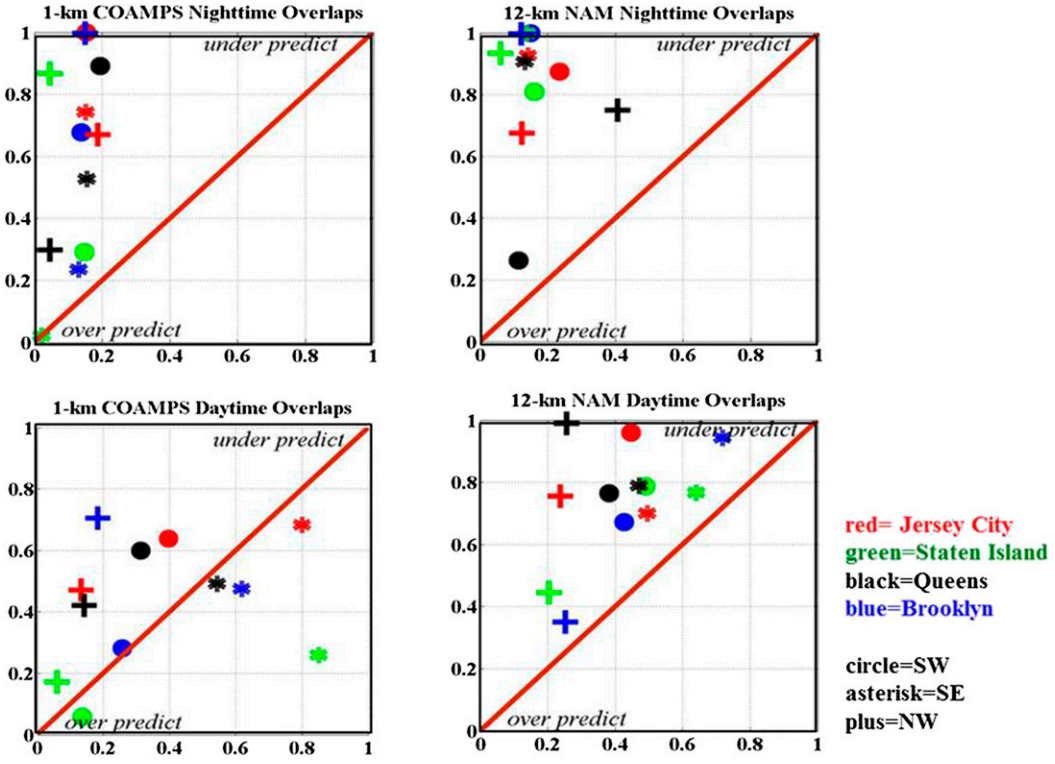

FIG. 13. Measure of effectiveness for COAMPS and NAM (both mode 4) for all wind directions and release sites. The control is mode 2 using 22 meteorological stations. Colors identify the release sites. Area of overlap divided by the area of the control plume is on the *x* axis; area of overlap divided by the area of meteorological-model plume is on the *y* axis.

As demonstrated in this study, understanding the transport of contaminants in an urban-coastal environment requires understanding the four-dimensional transport pathways within the BL. To improve plume predictions requires further consideration of *H* gradients and their contribution to atmospheric stability.

Fields produced by high-resolution atmospheric numerical models are complex and yield spatial and temporal variability often reflective of observed processes. Hence the coupling of high-resolution meteorological models and T&D models is of significant value. Efforts to link meteorological models to T&D models have been under way for several years (Wyszogrodzki et al. 2012; Miao et al. 2014; Kochanski et al. 2015). A caveat in this approach is that high-resolution models can be subject to a ''double penalty'' by producing small-scale features that are displaced in time or space or that are spurious in nature (Mass et al. 2002; Gilleland et al. 2009).

Because characterizing the state of the atmosphere always entails a degree of uncertainty, there is a pronounced need for sensor deployments to gather continuous quality-assured vertical BL measurements (radars, soundings, etc.). To be specific, sensors should be deployed in highly variable regions, such as the coastal zones surrounding the NY–NJ Harbor where release sites produce a broader range of plume outcomes. The nascent New York state mesonet is poised to contribute significantly to our monitoring and understanding of BL variability in the NY region.

Acknowledgments. We acknowledge the Defense Threat Reduction Agency for providing an academic access to HPAC software. We also acknowledge DTRA for providing funding for P. Bieringer's and G. Bieberbach's participation in this work through the Inter-Agency Cost Reimbursement Order B1144891 to NCAR and for providing access to the Hazard Prediction and Analysis Capability modeling software that was used in this study. The authors acknowledge the Research Applications Laboratory at NCAR for providing visiting-scientist travel support that helped to facilitate the technical collaborations in this work. The views expressed in this paper are solely those of the authors.

APPENDIX A

HPAC's Calculation and Parameters

SCIPUFF consists of two basic components: the dispersion-model equations and the turbulent-diffusion parameterization. This study deals closely with the

TABLE A1. Surface roughness estimation.

Z_0 (m)	Surface description
0.0005	Bare ground, sand dunes, water
0.001	Nearly barren with low growing vegetation
0.01	Grassland, cropland, wetlands
0.05	Grassland with scattered trees, bushland, scrub growth
0.1	Deciduous forest, villages, forest clearings
0.5	Mixed forest, towns, cities
1.0	Coniferous forest

specification of the planetary BL parameterization, which ultimately influences the calculations of the two terms mentioned above. The boundary layer in HPAC considers some idealizations of the BL structure in which the mean wind and turbulence are a function of 1) surface roughness, 2) surface friction velocity, 3) Monin–Obukhov length L, and 4) boundary layer depth. These parameters are not directly measurable quantities; HPAC therefore relates them to 1) reference velocity U_{ref}, 2) reference height Z_{ref}, and 3) sensible heat flux H.

The internal sequence of calculation is such that H is estimated first using a daytime and nighttime surface energy-balance method from Paine (1987). Unless variability is provided by a meteorological file, a constant H value, calculated at the release site, is applied across the entire grid and is then used to derive BL depth, convective velocity scale v, and friction velocity u_*. The combination of the four parameters (H, BL, v, and u_*), in addition to a referenced wind velocity, forms the vertical wind and turbulence profiles across the grid. HPAC allows for three different modes of BL calculations: "SIMPLE," "MET," and "CALCULATED." All three are used in this study and are explained in more detail below.

a. SIMPLE mode

Using HPAC's SIMPLE PBL mode, parameters are estimated using simple minimum and maximum values. For surface roughness z_0, HPAC uses estimation based on Saucier (1987), as given in Table A1. Surface friction velocity u_* (defined by the surface shear stress) is used to derive the wind and turbulence profiles and is given as

$$u_* = \frac{kU_{\text{ref}}}{\ln\left(\frac{Z_{\text{ref}}}{Z_0}+1\right)-\psi_m}.$$

Here, U_{ref} and Z_{ref} are constructed on the basis of the value of velocity at the lowest grid level and ψ_m is the stability-correction term. For neutral flow ($H = 0$), $\psi_m = 0$. For unstable conditions: ($L < 0$), ψ_m is given by

TABLE A2. Average Monin–Obukhov length and BL depth for different Pasquill–Gifford–Turner (PGT) stability classes (and the corresponding stability index).

Stability index	PGT class	L (m)	Z_i (m)
1	A, unstable	−5	1000
2	B, unstable	12.5	1000
3	C, unstable	−50	1000
4	D, neutral	−1000	1000
5	E, stable	25	125
6	F, stable	13	65
7	G, stable	5	25

$$\psi_m = 2\ln\left(\frac{1+\phi_m^{-1}}{2}\right)+\ln\left(\frac{1+\phi_m^{-2}}{2}\right)-2\tan^{-1}(\phi_m^{-1})+\frac{\pi}{2},$$

where the nondimensional velocity gradient is $\phi_m = [1-(15z/L)]^{-0.25}$. For stable conditions ($L > 0$), when $z < L$ then $\psi_m = -5z/L$ and when $z > L$ then

$$\psi_m = -17\left[1-\exp\left(-\frac{0.29z}{L}\right)\right].$$

In both cases,

$$\phi_m = 1+4.93\left(\frac{z}{L}\right)\exp\left(-\frac{0.29z}{L}\right).$$

The Monin–Obukhov length L accounts for the effects of atmosphere stability. An average Monin–Obukhov length is assumed within each stability index/class according to the method of Sykes and Lewellen (1992), as given in Table A2. Boundary layer height Z_i (Table A2) is set to 1000 m under neutral or unstable conditions and to $5L$ for stable conditions.

b. MET mode

Using HPAC's MET PBL mode, meteorological parameters provided by COAMPS and NAM are temperature profiles, wind profiles, sensible heat flux, boundary layer depth, surface friction velocity, surface roughness, relative humidity profile, and elevation.

c. CALCULATED mode

When HPAC's CALCULATED PBL mode is used, values are used when provided and the remaining parameters are calculated. Surface roughness, surface friction velocity, and Monin–Obukhov length are calculated the same way as they are in the SIMPLE mode.

Heat flux H is used to compute boundary layer depth, convective velocity scale, and friction velocity. HPAC computes the sensible heat flux using a surface energy-balance method similar to that found in "METPRO"

(Paine 1987). The method differs for daytime and nighttime. During the day

$$H = -\frac{u_*^3 T \rho_a c_p}{KgL},$$

where it is assumed that $L = 10Z_0$; u_* is calculated on neutral condition assumptions using Z_0, U_{ref}, and Z_{ref}; K is von Kármán's constant; T is the air temperature; ρ_a is the air density; c_p is the specific heat at constant pressure; and g is the gravitational acceleration. During the night, net incoming radiation is considered with total surface heat flux and is partitioned into sensible and latent components. The calculations require the input of fractional cloud cover, surface albedo, and Bowen ratio. Albedo, Bowen ratio, and cloud-cover values can be supplied or automated as in Paine (1987); net radiation calculations are provided to HPAC internally and were not able to be reproduced manually. The suggested values for surface albedo and Bowen ratio as a function of land use and season are based on Paine (1987). For this research, summer-month values for urban land use were applied as follows: albedo = 0.16, Bowen ratio = 2.0, and cloud cover = 0.5.

Boundary layer height Z_i is estimated on the basis of time of day. During the daytime, Z_i is calculated as in Kato and Phillips (1969):

$$Z_i = -2.5\frac{(Tu_*^3\rho_a c_p)}{0.2Hg}.$$

During the nighttime, $Z_i \approx L$. Once all parameters have been accounted for, HPAC will construct planetary boundary layer mean profiles. The wind mean profile is

$$u(z) = \left(\frac{u_*}{K}\right)\left[\ln\left(\frac{z}{z_{\text{surface}}}\right) - \psi_m\right],$$

where $z_{\text{surface}} = \alpha_{\text{surface}} z_i$, with

$$\alpha_{\text{surface}} = \begin{cases} 0.1 & L < 0 \\ 0.1 + 0.9\{(z_i/L)/[(z_i/L) + 5]\} & L > 0 \end{cases}.$$

For neutral and convective conditions, 0.1 is the estimate used by SCIPUFF, as based on Schumann (1988) and Wyngaard (1985).

The temperature mean profile is also calculated. The potential temperature gradient for stable conditions only is calculated as

$$T - T_0 = \frac{\theta_*}{K}\{0.74\ln[(z/z_0) + 1] - \psi_h\},$$

TABLE B1. Near-surface modeled winds in comparison with station wind data at the release sites, for winds from three directions: southwest (SW), northwest (NW), and southeast (SE). The comparison is expressed in terms of bias, with the first value in each cell being for the wind speed (in meters per second) and the second value being for wind direction (in degrees). Also given is the overlap (in percent), defined as the intersection areas of plumes derived from meteorological-model inputs (COAMPS and NAM) against control plumes calculated from observed near-surface winds and temperatures from station data.

	SW COAMPS		SW NAM		NW COAMPS		NW NAM		SE COAMPS		SE NAM	
	Wind bias	Overlap	Wind bias	Overlap	Wind bias	Overlap	Wind bias	Overlap	Wind bias	Overlap	Wind bias	Overlap
Jersey City day	−1.6, 31	40	−2.8, 1	45	−1.4, 13	13	−3.16, 73	24	2.5, 7	80	0.9, 15	50
Jersey City night	1.0, 29	16	−1.9, 37	23	0.5, 1	19	−3.07, 73	13	0.4, 58	15	−1.9, 2	14
Staten Island day	−1.9, 141	14	−1.9, 103	49	−1.7, 126	6	−3.73, 59	20	−3.2, 12	85	−5.5, 18	64
Staten Island night	−0.5, 120	15	−4.7, 100	16	−1.9, 3	5	−5.86, 14	6	−1.6, 15	2	−2.9, 48	14
Brooklyn day	−1.1, 141	26	−3.3, 7	43	−1.1, 61	18	−2.99, 56	25	1.9, 24	62	−0.8, 3	72
Brooklyn night	0.1, 7	14	−3.6, 20	15	2.4, 34	15	−1.28, 20	12	−0.3, 34	13	−2.9, 29	15
Queens day	0.5, 35	13	−2.4, 10	38	0.1, 34	14	−2.23, 36	26	0.5, 4	54	−0.9, 36	47
Queens night	−0.48, 34	20	−3.9, 57	12	−0.7, 61	5	−3.36, 71	41	−1.1, 25	15	−3.9, 26	13

where $\theta_* = -H/(\rho_a c_p u_*)$ and $\psi_h = -4.7Z/L$. The gradient is assumed to be zero for neutral and convective conditions, since the potential temperature is well mixed. Another variable that is calculated is the convective velocity scale w_*. From Deardorff (1970), the convective velocity scale, which dominates the turbulence calculations in HPAC, is defined as

$$w_* = \left(\frac{gHz_i}{T\rho_a c_p}\right)^{1/3}$$

and can be related to L by

$$\frac{L}{z_i} = -\frac{u_*^3}{kw_*^3}.$$

APPENDIX B

Meteorological Specifications and Comparison Statistics

COAMPS and NAM wind magnitude and direction are compared with the observed winds at the release location at the same date/time (daytime is 1300 local time, and nighttime is 0100 local time) using bias statistics. Comparison statistics (percent overlap) are also given for the resultant plumes (mode 4) in relation to the control (mode 2) plumes. Table B1 gives the results for these bias and overlap comparisons.

REFERENCES

Allwine, K. J., and J. E. Flaherty, 2006a: Joint Urban 2003: Study overview and instrument locations. Pacific Northwest National Laboratory Rep. PNNL-15967, 91 pp. [Available online at https://www.pnl.gov/main/publications/external/technical_reports/PNNL-15967.pdf.]

——, and ——, 2006b: Urban dispersion program MSG05 field study: Summary of tracer and meteorological measurements. Pacific Northwest National Laboratory Rep. PNNL-15969, 26 pp. [Available online at http://www.pnl.gov/main/publications/external/technical_reports/PNNL-15969.pdf.]

——, and ——, 2007: Urban dispersion program overview and MID05 field study summary. Pacific Northwest National Laboratory Rep. PNNL-16696, 62 pp. [Available online at https://www.pnl.gov/main/publications/external/technical_reports/PNNL-16696.pdf.]

——, J. H. Shinn, G. E. Streit, K. L. Clawson, and M. Brown, 2002: Overview of URBAN 2000: A multiscale field study of dispersion through an urban environment. *Bull. Amer. Meteor. Soc.*, **83**, 521–536, doi:10.1175/1520-0477(2002)083<0521:OOUAMF>2.3.CO;2.

Bass, A., 1980: Modeling long range transport and diffusion. Preprints, *Second Joint Conf. on Applications of Air Pollution Meteorology*, New Orleans, LA, Amer. Meteor. Soc. and Air Pollution Control Association, 193–215.

Bornstein, R. D., 1968: Observations of the urban heat island effect in New York City. *J. Appl. Meteor.*, **7**, 575–582, doi:10.1175/1520-0450(1968)007<0575:OOTUHI>2.0.CO;2.

——, and D. S. Johnson, 1977: Urban–rural wind velocity differences. *Atmos. Environ.*, **11**, 597–604, doi:10.1016/0004-6981(77)90112-3.

——, and Q. Lin, 2000: Urban heat islands and summertime convective thunderstorms in Atlanta: Three case studies. *Atmos. Environ.*, **34**, 507–516, doi:10.1016/S1352-2310(99)00374-X.

Brown, M. J., 2004: Urban dispersion—Challenges for fast response modeling. *Fifth Conf. on Urban Environment*, Vancouver, BC, Canada, Amer. Meteor. Soc., J5.1. [Available online at https://ams.confex.com/ams/pdfpapers/80330.pdf.]

——, and M. D. Williams, 1998: An urban canopy parameterization for mesoscale meteorology models. Preprints, *Second Urban Environment Symp.*, Albuquerque, NM, Amer. Meteor. Soc., 144–147.

Chang, J. C., S. R. Hanna, Z. Boybeyi, and P. Franzese, 2005: Use of Salt Lake City URBAN 2000 field data to evaluate the Urban Hazard Prediction Assessment Capability (HPAC) dispersion model. *J. Appl. Meteor.*, **44**, 485–501, doi:10.1175/JAM2205.1.

Chin, H.-N. S., M. J. Leach, G. A. Sugiyama, J. M. Leone Jr., H. Walker, J. S. Nasstrom, and M. J. Brown, 2005: Evaluation of an urban canopy parameterization in a mesoscale model using VTMX and URBAN 2000 data. *Mon. Wea. Rev.*, **133**, 2043–2068, doi:10.1175/MWR2962.1.

Cummings, J. A., 2005: Operational multivariate ocean data assimilation. *Quart. J. Roy. Meteor. Soc.*, **131**, 3583–3604, doi:10.1256/qj.05.105.

Deardorff, J. W., 1970: Convective velocity and temperature scales for the unstable planetary boundary layer and for Rayleigh convection. *J. Atmos. Sci.*, **27**, 1211–1213, doi:10.1175/1520-0469(1970)027<1211:CVATSF>2.0.CO;2.

Donaldson, C. du P., 1973: Atmospheric turbulence and the dispersal of atmospheric pollutants. *Workshop on Micrometeorology*, D. A. Haugen, Ed., Amer. Meteor. Soc., 313–390.

DTRA, 2008: *Hazard Prediction and Assessment Capability (HPAC) version 5.0 SP1.* Defense Threat Reduction Agency, DVD. [Available from Defense Threat Reduction Agency, 8725 John J. Kingman Rd., MSC 6201, Ft. Belvoir, VA 22060-6201.]

Galmarini, S., R. Bianconi, R. Bellasio, and G. Graziani, 2001: Forecasting the consequences of accidental releases of radionuclides in the atmosphere from ensemble dispersion modelling. *J. Environ. Radioact.*, **57**, 203–219, doi:10.1016/S0265-931X(01)00017-0.

Garten, J. F., C. E. Schemm, and A. R. Croucher, 2003: Modeling the transport and dispersion of airborne contaminants: A review of techniques and approaches. *Johns Hopkins APL Technical Digest*, Vol. 24, Johns Hopkins Applied Physics Laboratory, Laurel, MD, 368–375. [Available online at http://www.jhuapl.edu/techdigest/TD/td2404/Garten.pdf.]

Gedzelman, S. D., S. Austin, R. Cermak, N. Stefano, S. Partridge, S. Quesenberry, and D. A. Robinson, 2003: Mesoscale aspects of the urban heat island around New York City. *Theor. Appl. Climatol.*, **75** , 29–42, doi:10.1007/s00704-002-0724-2.

Gilleland, E., D. Ahijevych, B. G. Brown, B. Casati, and E. E. Ebert, 2009: Intercomparison of spatial forecast verification methods. *Wea. Forecasting*, **24**, 1416–1430, doi:10.1175/2009WAF2222269.1.

Hanna, S., and J. Chang, 2012: Acceptance criteria for urban dispersion model evaluation. *Meteor. Atmos. Phys.*, **116**, 133–146, doi:10.1007/s00703-011-0177-1.

——, and ——, 2015: Skyscraper rooftop tracer concentration observations in Manhattan and comparisons with urban

dispersion models. *Atmos. Environ.*, **106**, 215–222, doi:10.1016/j.atmosenv.2015.01.051.

——, ——, J. White, and J. Bowers, 2008: Evaluation of the Hazard Prediction and Assessment Capability (HPAC) model with the Oklahoma City Joint Urban 2003 (JU2003) tracer observations. *Air Pollution Modeling and Its Application XIX*, C. Borrego and A. I. Miranda, Eds., Springer, 63–71. [Available online at http://link.springer.com/chapter/10.1007%2F978-1-4020-8453-9_7.]

——, I. Sykes, S. Parker, J. Chang, J. M. White, and E. Baja, 2009: Urban HPAC/SCIPUFF and a simple urban dispersion model compared with the Madison Square Garden 2005 tracer observations in New York City. *Eighth Symp. on the Urban Environment*, Phoenix, AZ, Amer. Meteor. Soc., J18.2. [Available online at https://ams.confex.com/ams/pdfpapers/146811.pdf.]

——, and Coauthors, 2011: Comparisons of JU2003 observations with four diagnostic urban wind flow and Lagrangian particle dispersion models. *Atmos. Environ.*, **45**, 4073–4081, doi:10.1016/j.atmosenv.2011.03.058.

Hodur, R. M., 1997: The Naval Research Laboratory's Coupled Ocean/Atmosphere Mesoscale Prediction System (COAMPS). *Mon. Wea. Rev.*, **125**, 1414–1430, doi:10.1175/1520-0493(1997)125<1414:TNRLSC>2.0.CO;2.

Holt, T. R., and J. Pullen, 2007: Urban canopy modeling of the New York City metropolitan area: A comparison and validation of single- and multilayer parameterizations. *Mon. Wea. Rev.*, **135**, 1906–1930, doi:10.1175/MWR3372.1.

Janjić, Z. I., J. P. Gerrity Jr., and S. Nickovic, 2001: An alternative approach to nonhydrostatic modeling. *Mon. Wea. Rev.*, **129**, 1164–1178, doi:10.1175/1520-0493(2001)129<1164:AAATNM>2.0.CO;2.

Kato, H., and O. M. Phillips, 1969: On the penetration of a turbulent layer into a stratified fluid. *J. Fluid Mech.*, **37**, 643–655, doi:10.1017/S0022112069000784.

Keim, B. D., L. D. Meeker, and J. F. Slater, 2005: Manual synoptic climate classification for the east coast of New England (USA) with an application to $PM_{2.5}$ concentration. *Climate Res.*, **28**, 143–153, doi:10.3354/cr028143.

Kochanski, A. K., E. R. Pardyjak, R. Stoll, A. Gowardhan, M. J. Brown, and W. J. Steenburgh, 2015: One-way coupling of the WRF–QUIC urban dispersion modeling system. *J. Appl. Meteor. Climatol.*, **54**, 2119–2139, doi:10.1175/JAMC-D-15-0020.1.

Lewellen, W. S., 1977: Use of invariant modeling. *Handbook of Turbulence*, W. Frost and T. H. Moulden, Eds., Plenum Press, 237–280.

Liu, Y., F. Chen, T. Warner, and J. Basara, 2006: Verification of a mesoscale data-assimilation and forecasting system for the Oklahoma City area during the Joint Urban 2003 field project. *J. Appl. Meteor. Climatol.*, **45**, 912–929, doi:10.1175/JAM2383.1.

Mahrer, Y., and R. A. Pielke, 1977: The effects of topography on sea and land breezes in a two-dimensional numerical model. *Mon. Wea. Rev.*, **105**, 1151–1162, doi:10.1175/1520-0493(1977)105<1151:TEOTOS>2.0.CO;2.

Mass, C. F., D. Ovens, K. Westrick, and B. A. Colle, 2002: Does increasing horizontal resolution produce more skillful forecasts? The results of two years of real-time numerical weather prediction over the Pacific Northwest. *Bull. Amer. Meteor. Soc.*, **83**, 407–430, doi:10.1175/1520-0477(2002)083<0407:DIHRPM>2.3.CO;2.

Meir, T., P. M. Orton, J. Pullen, T. Holt, W. T. Thompson, and M. F. Arend, 2013: Forecasting the New York City urban heat island and sea breeze during extreme heat events. *Wea. Forecasting*, **28**, 1460–1477, doi:10.1175/WAF-D-13-00012.1.

Miao, Y., S. Liu, H. Zheng, Y. Zheng, B. Chen, and S. Wang, 2014: A multi-scale urban atmospheric dispersion model for emergency management. *Adv. Atmos. Sci.*, **31**, 1353–1365, doi:10.1007/s00376-014-3254-9.

National Research Council, 2001: Standing operating procedures for developing acute exposure guideline levels for hazardous chemicals. National Research Council Rep., 224 pp. [Available online at https://www.epa.gov/sites/production/files/2015-09/documents/sop_final_standing_operating_procedures_2001.pdf.]

Paine, R. J., 1987: User's guide to the CTDM meteorological preprocessor (METPRO) program. U.S. Environmental Protection Agency Project Rep. EPA/600/8-88/004, 161 pp. [Available online at https://nepis.epa.gov/.]

Pullen, J., T. Holt, A. F. Blumberg, and R. D. Bornstein, 2007: Atmospheric response to local upwelling in the vicinity of New York–New Jersey Harbor. *J. Appl. Meteor. Climatol.*, **46**, 1031–1052, doi:10.1175/JAM2511.1.

Rodriguez, L. M., P. E. Bieringer, and T. Warner, 2013: Urban transport and dispersion model sensitivity to wind direction uncertainty and source location. *Atmos. Environ.*, **64**, 25–39, doi:10.1016/j.atmosenv.2012.08.037.

Saucier, R., 1987: NUSSE3 model description. U.S. Army Chemical Research, Development and Engineering Center Rep. CRDEC-TR-87046.

Schumann, U., 1988: Minimum friction velocity and heat transfer in the rough surface layer of a convective boundary layer. *Bound.-Layer Meteor.*, **44**, 311–326, doi:10.1007/BF00123019.

Sykes, R. I., and W. S. Lewellen, 1992: Review of potential models for UF_6 dispersion. Martin Marietta Energy Systems, Inc., Rep. K/GDP/SAR-19, 77 pp.

——, S. Parker, D. Henn, and B. Chowdhury, 2007: SCIPUFF version 2.3 technical documentation. L-3 Technologies, Inc., Rep., 336 pp.

Thompson, W. T., T. Holt, and J. Pullen, 2007: Investigation of a sea breeze front in an urban environment. *Quart. J. Roy. Meteor. Soc.*, **133**, 579–594, doi:10.1002/qj.52.

Warner, S., N. Platt, and J. F. Heagy, 2004a: Comparisons of transport and dispersion model predictions of the URBAN 2000 field experiment. *J. Appl. Meteor.*, **43**, 829–846, doi:10.1175/1520-0450(2004)043<0829:COTADM>2.0.CO;2.

——, ——, and ——, 2004b: User-oriented two-dimensional measure of effectiveness for the evaluation of transport and dispersion models. *J. Appl. Meteor.*, **43**, 58–73, doi:10.1175/1520-0450(2004)043<0058:UTMOEF>2.0.CO;2.

——, ——, ——, J. E. Jordan, and G. Bieberbach, 2006: Comparisons of transport and dispersion model predictions of the Mock Urban Setting Test field experiment. *J. Appl. Meteor. Climatol.*, **45**, 1414–1428, doi:10.1175/JAM2410.1.

White, J. M., J. F. Bowers, S. R. Hanna, and J. K. Lundquist, 2009: Importance of using observations of mixing depths in order to avoid large prediction errors by a transport and dispersion model. *J. Atmos. Oceanic Technol.*, **26**, 22–32, doi:10.1175/2008JTECHA1134.1.

Wyngaard, J. C., 1985: Structure of the planetary boundary layer and implications for its modeling. *J. Climate Appl. Meteor.*, **24**, 1131–1142, doi:10.1175/1520-0450(1985)024<1131:SOTPBL>2.0.CO;2.

Wyszogrodzki, A. A., S. Miao, and F. Chen, 2012: Evaluation of the coupling between mesoscale-WRF and LES-EULAG models for simulating fine-scale urban dispersion. *Atmos. Res.*, **118**, 324–345, doi:10.1016/j.atmosres.2012.07.023.